

Direct Observation of Spin Current Oscillation in a Ferromagnet

Mengyao Du,^{1,*} Huiqian Min^{1,*}, Ke Xia,² Dazhi Hou,³ Lei Wang⁴, and Zhiyong Qiu^{1,†}


¹Key Laboratory of Materials Modification by Laser, Ion, and Electron Beams, Ministry of Education, School of Materials Science and Engineering, *Dalian University of Technology*, Dalian, 116024, China

and Key Laboratory of Energy Materials and Devices, Liaoning Province, School of Materials Science and Engineering, *Dalian University of Technology*, Dalian, 116024 Liaoning, China

²School of Physics, *Southeast University*, Nanjing 211189, China

³ICQD, Hefei National Laboratory for Physical Sciences at Microscale, *University of Science and Technology of China*, Hefei, Anhui 230026, China and Department of Physics, *University of Science and Technology of China*, Hefei, Anhui 230026, China

⁴Key Laboratory of Quantum Materials and Devices of Ministry of Education, School of Physics, *Southeast University*, Nanjing 211189, China

 (Received 30 May 2023; revised 5 December 2023; accepted 26 January 2024; published 14 June 2024)

Spin current is a crucial element in spintronics, and its diffusion in materials is typically characterized by monotonic decay. However, when the material hosting the spin current is also a magnet, the spin current is expected to exhibit spatial oscillations, the observation of which remains elusive. Here, we demonstrate the spatial oscillation of a spin current in a nickel film by measuring the thickness-dependent inverse spin Hall effect in Ni/YIG bilayers. The inverse spin Hall current in nickel is found to oscillate with its film thickness, in contrast to nonmagnetic materials, and that the oscillation period quantitatively agrees with theoretical predictions based on differences in the Fermi wave vector between majority and minority carriers. Our findings reveal a previously hidden behavior of spin-transport dynamics and identify a new degree of freedom for manipulating spin current, with potential implications for future spintronic devices.

DOI: [10.1103/PhysRevX.14.021045](https://doi.org/10.1103/PhysRevX.14.021045)

Subject Areas: Condensed Matter Physics, Spintronics

I. INTRODUCTION

Spin transport in magnetic materials has attracted significant research interest due to the intricate interplay between the magnetic structure and transport properties. Specifically, the transport of spins perpendicular to the film plane gives rise to numerous physical effects, such as the giant magnetoresistance effect [1,2], tunnel magnetoresistance [3,4], spin-transfer torque (STT) [5,6], and spin-orbit torque [7,8]. Since the majority (\uparrow) and minority (\downarrow) electrons on the Fermi surface do not share the same wave vector and the two states are usually coherent, there is theoretical consensus that suggests spins propagating in a ferromagnet experience a spatial precession [9–15]. The spatial precession “wave vector” is $\Delta k_F = k_F^\uparrow - k_F^\downarrow$, while the precession wavelength is $\lambda = 2\pi/|k_F^\uparrow - k_F^\downarrow|$ (Fig. 1) [11–14]. Such a precession may be detected as a spatial

oscillation of STT or spin current density, which will vary by distance from an interface [14,16]. However, the observation of the spatial precession of propagating spins has remained elusive due to the strong decoherence effect in ferromagnetic metals. The spin-splitting energies are typically of the same order as the Fermi energy for most transition metals, leading to coherence lengths ($\lambda_c = \pi/|k_F^\uparrow - k_F^\downarrow|$) that are comparable to the unit-cell dimension, which is challenging for the measurement of spin precession [11–14]. Moreover, the spin current has the contribution from all wave vectors at the Fermi surface [12]. Because of the complex structure of the Fermi surface of high-electron-density metallic ferromagnets such as cobalt and iron, the frequencies of those wave vectors show a large span of magnitude. Therefore, although each k_F point involves a strongly oscillating integrand, the integral of the Fermi surface at a distance d should be canceled out due to the destructive interference, except for very small values of d [11–13]. Furthermore, most studied systems bear an intrinsic disadvantage in the observation of spin precession [17,18]. Atomic-scale disorder, especially at interfaces, is another non-negligible reason for the phase decoherence of the spin-resolved electron waves. Thus, it has been considered reasonable to treat spin currents in a semiclassical (or quasiclassical) framework in a metallic

*These authors contributed equally to this work.

†Corresponding author: qiuzy@dlut.edu.cn

Published by the American Physical Society under the terms of the [Creative Commons Attribution 4.0 International license](https://creativecommons.org/licenses/by/4.0/). Further distribution of this work must maintain attribution to the author(s) and the published article’s title, journal citation, and DOI.

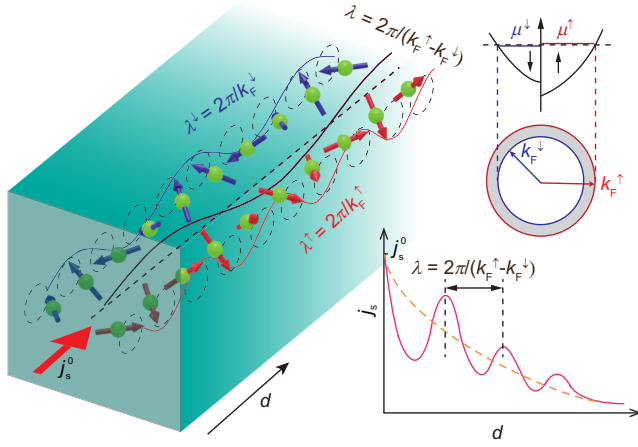


FIG. 1. Illustration of the spin precession along the thickness direction and the band structure of Ni. The graph displays the spatial precession of electrons in a nickel film with different spin-up (k_F^\uparrow) and spin-down (k_F^\downarrow) wave vectors, along with their associated coherent processes. This difference in wave vectors leads to a periodic oscillation of the spin current intensity along the thickness d direction, with a period given by $\lambda = 2\pi/|k_F^\uparrow - k_F^\downarrow|$. j_s refers to the spin current density, and j_s^0 is the spin current density at the interface.

system. In this context, spin-spin interference is localized very close to the interface of spin injection, and spin current is treated as a diffusive particle flow [12–15,19–21].

On the other hand, several authors have suggested that some weak ferromagnets, including nickel and diluted magnetic semiconductors (e.g., GaMnAs), which exhibit much smaller spin-splitting energy than most 3d transition metals, might enhance the coherence length λ_c [13,22,23]. In particular, nickel has been suggested to be a potential candidate to probe the spin-spin coherence phenomenon which was explored in independent theoretical studies conducted by Carva and Turek and Wang *et al.*, with respect to the concepts of spin-mixing conductance and STT, respectively [13,14]. Both works suggest that the spin-coherence length λ_c of nickel should be extensive due to the small average Δk_F between majority and minority spins. Moreover, the similar symmetry of the Fermi surfaces between majority and minority spins—resulting in the propagating states with similar precession wave vector Δk_F —suppresses the cancellation among different wave vectors. Thus, the spin-related oscillation in nickel should be more significant than other 3d ferromagnetic elements. The oscillation periods aligned with the (110) and (111) directions have been quantitatively calculated [13,14]. However, to date, no experimental evidence has been found to confirm this expected spin precession in magnets.

II. EXPERIMENTAL SETUP AND RESULTS

In this work, spin transport in metallic nickel films is studied systematically by using a spin-pumping technique

[24]. The yttrium iron garnet (YIG)/nickel (Ni) bilayer devices with various nickel layer thicknesses are fabricated to achieve high interface and bulk quality. Spin accumulation is excited by the spin-pumping effect at the YIG/Ni interface, and then a spin current is injected into the nickel layer where it is converted into a charge current by the inverse spin Hall effect (ISHE) [25,26]. Surprisingly, a clear thickness-dependent oscillation is observed in the ISHE signals, which reflects the spin-coherent precession of the propagating spin.

The bilayer spin-pumping devices used in this work were composed of an insulating YIG layer and a metallic nickel layer. High-quality single-crystal YIG was grown on a $\text{Gd}_3\text{Ga}_5\text{O}_{12}$ wafer by using a liquid-phase epitaxy method with a thickness about 3 μm . Subsequently, samples, size $1.5 \times 3 \text{ mm}^2$, were cut from the same wafer. Nickel layers, ranging in thickness from 1 to 15 nm, were deposited on the YIG layer using a high-vacuum magnetron-sputtering system, with strict control of the deposition conditions to ensure consistency in the interfaces and bulk qualities of all samples.

Figure 2(a) shows typical x-ray-diffraction patterns of the YIG/Ni bilayer device. Besides the strongest peak from the YIG substrate, the only peak corresponding to the (111) crystal plane of the face-centered-cubic nickel can be confirmed, which suggests that the nickel layer exhibits a highly (111)-preferential orientation. The grain size is estimated to be about 15.7 nm, as calculated using the Scherrer equation [27], which is comparable to the nickel layer thickness. These results suggest that the nickel layers in the YIG/Ni bilayer devices are of good crystalline quality with highly (111)-oriented structures. The x-ray-reflectivity spectrum for a typical YIG/Ni bilayer device with a 10-nm-thick nickel layer is shown in Fig. 2(b), and it is well represented by a simulation. The surface and interface roughnesses are estimated to be about 0.16 and 0.26 nm, respectively, which implies uniform surface and interface in our samples. The nickel layer thicknesses of all samples are well controlled, with an error margin of ± 0.15 nm. The inset of Fig. 2(c) presents a cross-sectional TEM image of a YIG/Ni bilayer device. Owing to a marked mismatch between the YIG and Ni lattices, the nickel film does not grow epitaxially from the YIG lattice. Nevertheless, the interface between YIG and Ni exhibits an atomically smooth transition, with the transition layer falling below several atomic layers. Importantly, no discernible diffusion layer can be observed. The image clearly demonstrates that the Ni layer maintains a high degree of crystallographic integrity and a preferred orientation, which are fundamental prerequisites for observing the spatial oscillation of spin in our study.

Transverse resistivities ρ of all YIG/Ni bilayer devices were measured using a four-terminal method wherein the nickel layers were shaped into six-terminal Hall-bar structures. ρ of all YIG/Ni bilayer devices is shown in Fig. 2(c). With the increasing nickel layer thickness d_{Ni} , the

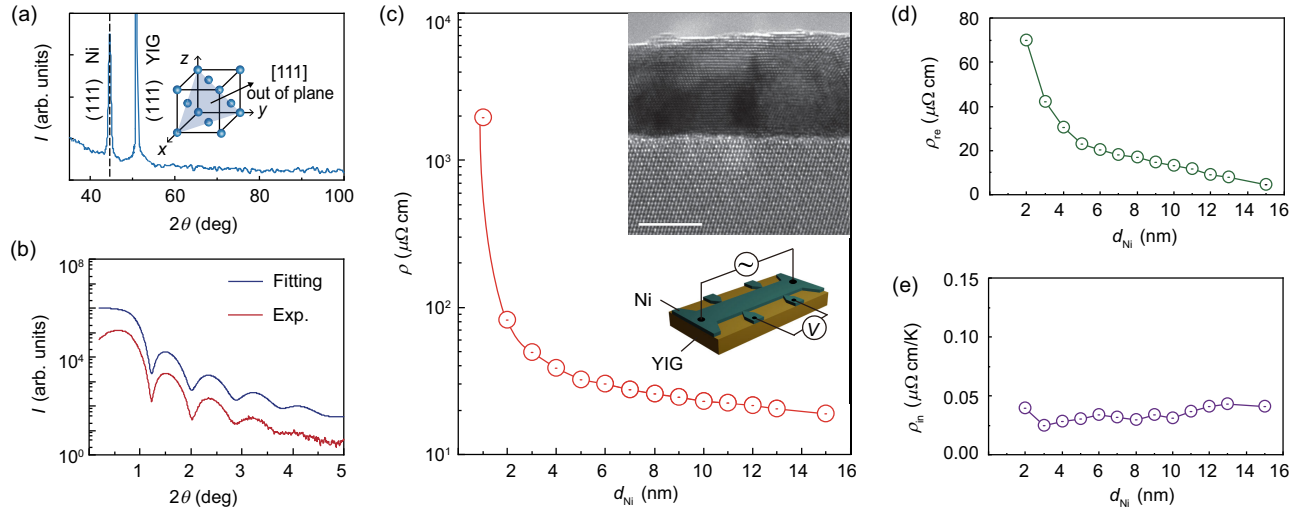


FIG. 2. Characterizations of the YIG/Ni bilayer devices. (a) The x-ray-diffraction patterns. (b) The x-ray-reflectivity spectrum and its fitting result of a device with a 10-nm-thick nickel layer. (c) The transverse resistivity ρ dependence on the nickel layer thickness d_{Ni} , as determined by a four-terminal measurement setup. The insets are cross-sectional TEM images of the YIG/Ni sample and experiment setup; scale bar = 2 nm. (d) Residual resistivity ρ_{re} dependence on the nickel layer thickness d_{Ni} . (e) Temperature coefficient dependence on the nickel layer thickness d_{Ni} of ρ_{in} .

resistivities ρ decrease monotonically and smoothly, which indicates that the thicknesses and qualities of the nickel layers are well controlled. Furthermore, the transverse resistivity ρ can be related to the temperature T as $\rho = \rho_{\text{re}} + \rho_{\text{in}}T$ [28]. Here, ρ_{re} and ρ_{in} refer to the residual resistivity and the temperature coefficient of resistivity, which reflect the contribution of extrinsic scattering and the intrinsic bound structure, respectively. In Figs. 2(d) and 2(e), ρ_{re} and ρ_{in} are shown depending on the nickel layer thicknesses d_{Ni} , which are estimated from the temperature-dependent measurement. It is found that ρ_{re} shows a strong thickness dependence, dominating the differences of resistivities ρ in various YIG/Ni bilayer devices. This suggests that the surface and interface scattering for itinerant electrons are the dominant factors for the resistivity ρ , which are weaker with a thicker nickel layer thickness d_{Ni} . On the other hand, ρ_{in} is almost stable for all samples with different nickel layer thicknesses d_{Ni} , confirming that the bulk qualities of all nickel layers are comparable [Fig. 2(e)].

A spin-pumping setup was used to study the ISHE of nickel in YIG/Ni bilayer devices. The sample was directly placed onto the signal line of a coplanar waveguide, as shown in Fig. 3(a). By applying a microwave and an external magnetic field, spin accumulation was excited at the YIG/Ni interface, and spin currents were pumped into the nickel layer. The detectable transverse voltage signals arose from the ISHE of the nickel layers, in accordance with the theoretical model of the spin-pumping effect [26].

The transverse voltage signals have been well studied and discussed depending on the nickel layer thicknesses d_{Ni} . Figure 3(b) shows a typical magnetic field H dependence of microwave power P for the YIG/Ni bilayer device at $T = 300$ K, under a microwave frequency $f = 5$ GHz.

Two obvious absorption peaks symmetrically appear at magnetic fields $H_{\text{FMR}} \approx \pm 0.12$ T, which refers to the ferromagnetic resonance (FMR) condition for the YIG layer. All YIG/Ni bilayer devices have the same FMR fields because all YIG have the same quality and come from the same wafer. The magnetic field H dependences of transverse voltage signals V for the samples with different nickel layer thicknesses d_{Ni} are shown in Fig. 3(c). Here, microwave absorption powers P_{ab} for all samples are carefully kept at the same level. Clear voltage peaks can be observed at the same positions of the FMR field H_{FMR} for all samples. The signs of those voltage peaks are reversed by reversing the magnetic field H . This correlates well with the theory of the spin-pumping effect, which indicates that the voltage peaks are the converted ISHE signals of the spin currents pumped from the YIG layer [26]. Here, we define the height of these voltage peaks as the ISHE signals V_{ISHE} [Fig. 2(c)], and the ratio between V_{ISHE} and the resistivity R is the ISHE current I_{ISHE} .

The V_{ISHE} for all samples with different nickel layer thicknesses d_{Ni} is comparably shown in Fig. 2(c). It is surprising that the V_{ISHE} does not decrease monotonically as predicted by the spin-pumping theory [26], but oscillates up and down with an increasing nickel layer thickness d_{Ni} . As depicted by the dependence of I_{ISHE} on nickel layer thickness d_{Ni} in Fig. 3(d), the I_{ISHE} exhibits a distinct oscillation with a period of about 3 nm. Similar oscillations are observed throughout a broad temperature range as detailed in the Supplemental Material [29]. Even the overall trend of the I_{ISHE} seems to follow the prediction of the present spin-pumping theory [26], and the oscillation cannot be explained without taking a spin-coherent effect into consideration.

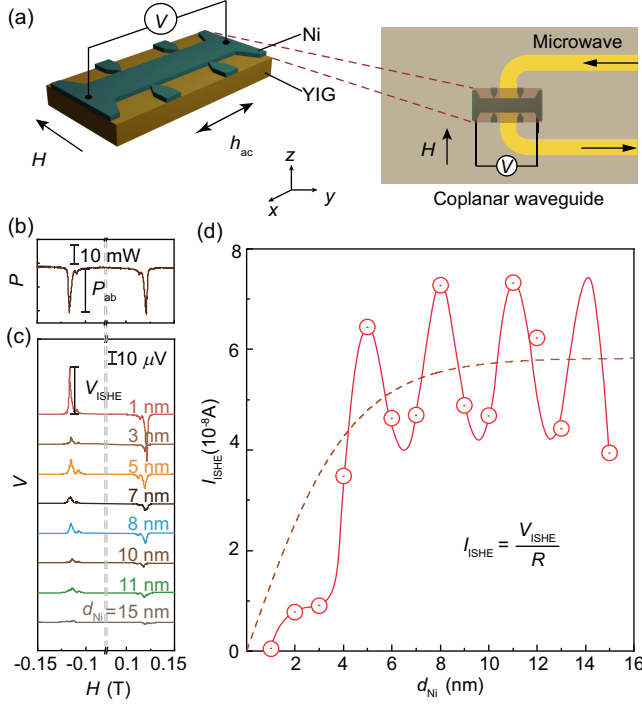


FIG. 3. The experiment setup and the result of the spin-pumping measurement. (a) The schematic of the YIG/Ni bilayer device and the experimental setup for the spin-pumping measurement. (b) A microwave absorption spectrum for a YIG/Ni bilayer device at $T = 300$ K. (c) The dependences of the voltage signals V_{ISHE} on the external magnetic field H for the YIG/Ni bilayer devices with various nickel layer thicknesses d_{Ni} at $T = 300$ K. (d) The nickel layer thickness d_{Ni} dependence of I_{ISHE} for the YIG/Ni bilayer devices at $T = 300$ K. Here, the lines are guides for the eyes.

III. DISCUSSION

Insight into this spin current oscillation can be obtained through the discussion of STT. Wang *et al.* [14] previously suggested that STT in nickel could be attributed to two components. The first component is comprised of propagating states with a spatial precession wave vector $\Delta k_{\text{F}} = k_{\text{F}}^{\uparrow} - k_{\text{F}}^{\downarrow}$, which arises due to spin coherence between majority and minority spins. The second component is due to the decay of spins caused by scattering, and this phenomenon was also considered in developing the spin-pumping theory. Since the intensity of STT is almost directly proportional to the transverse component of the incident spin current [10], we can directly use Wang's formula to explain the spin current oscillation in this study. Therefore, the inverse spin Hall signal V_{ISHE} can be expressed as the sum of the oscillation term V_{osc} and the decay term V_{dec} as follows:

$$V_{\text{ISHE}} = V_{\text{dec}} + V_{\text{osc}}. \quad (1)$$

The decay term has the same form as used in spin-pumping theory [26] and is given by

$$V_{\text{dec}} = wR\theta_{\text{SHE}}\lambda \tanh\left(\frac{d_{\text{Ni}}}{2\lambda}\right) \left(\frac{2e}{\hbar}\right) j_{\text{s}}^0. \quad (2)$$

Here, w , R , θ_{SHE} , and λ represent the width, resistance, spin Hall angle, and spin-diffusion length of the nickel layer, respectively. j_{s}^0 refers to the spin current density at the YIG/Ni interface for the decay term. For the oscillation term, following Refs. [10,14], the spin current density $j_{\text{s}}(z)$ along the normal direction (z) of the thin film of nickel can be expressed as

$$j_{\text{s}}^{\text{ISHE}}(z) = A \text{Im}\{e^{i(\Delta k_{\text{F}} \times z + \phi)}\}, \quad (3)$$

where the parameters A and ϕ represent the intensity coefficient and initial phase of the coherent spin current density, respectively. These parameters determine the spin current out of the YIG/Ni interface. The corresponding inverse spin Hall current density is determined by $j_{\text{c}}^{\text{ISHE}}(z) = (2e/\hbar)\theta_{\text{SHE}}j_{\text{s}}(z)$. By averaging the current density over the whole thickness d_{Ni} of Ni, the corresponding oscillation voltage will be

$$\begin{aligned} V_{\text{osc}} &= wR \int_0^{d_{\text{Ni}}} j_{\text{c}}^{\text{ISHE}}(z) dz \\ &= -\frac{2e}{\hbar} \frac{AwR\theta_{\text{SHE}}}{\Delta k_{\text{F}}} \text{Re}\{e^{i(\Delta k_{\text{F}} \times d_{\text{Ni}} + \phi)} - e^{i\phi}\}. \end{aligned} \quad (4)$$

Moreover, as we already have an unknown parameter A , we can simplify the above equation as

$$V_{\text{osc}} = \frac{RP}{\Delta k_{\text{F}}} \text{Re}\{e^{i(\Delta k_{\text{F}} \times d_{\text{Ni}} + \phi)}\} + V_0. \quad (5)$$

The inverse spin Hall voltage V_{ISHE} dependence on the nickel layer thickness d_{Ni} can be well represented by Eq. (1) [Fig. 4(a)] if we consider \mathcal{P} , ϕ , w , θ_{SHE} , V_0 , and λ as constants. The fitted terms of V_{osc} and V_{dec} are shown in Figs. 4(b) and 4(c), respectively. It is apparent that the first term of V_{osc} exhibits significant oscillation depending on the thickness of the nickel layer. The predicted wavelength of about 2.95 nm for the spin precession along the (111) direction in nickel (14.5 ML) [14] is consistent with the observed wavelength of about 3.03 nm. The amplitude decay can primarily be attributed to the transverse resistivity of those samples, which agrees with the slow decay and long spin-coherence length in nickel [13,14]. On the other hand, the second decay term agrees well with the present spin-pumping theory, in which the spin current is described by a diffusion function. This finding suggests that the scattering mechanism is still the primary factor for spin transport in nickel. The spin-diffusion length—a characteristic length that describes the spatial decay of the spin polarization—can be estimated to be about 2.15 nm, which is consistent with data from other groups [30]. The value of $\theta_{\text{SHE}}j_{\text{s}}^0(2e/\hbar)$ is almost 12.5 times larger

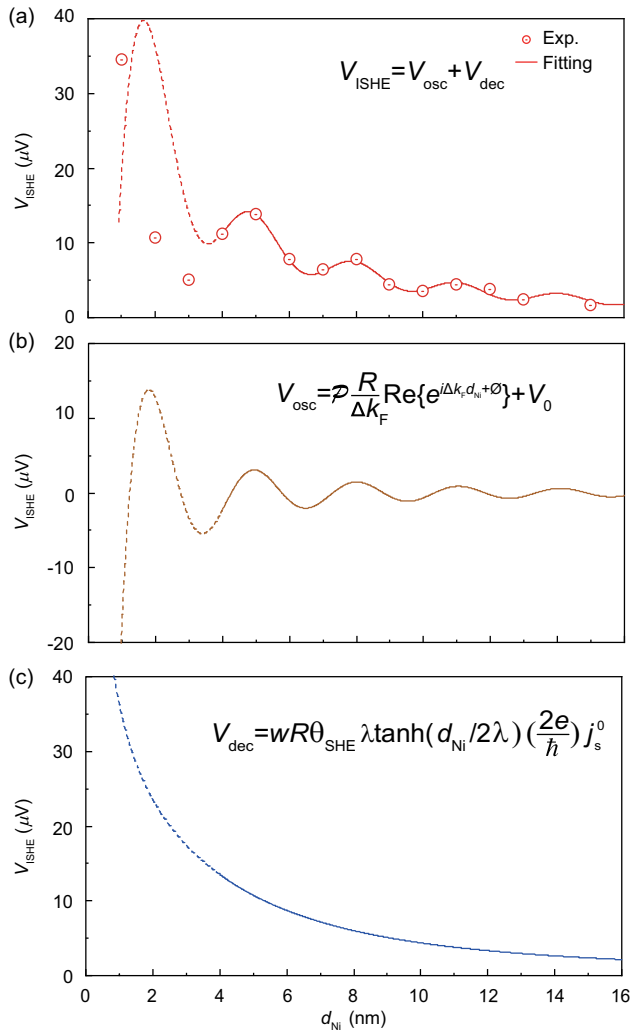


FIG. 4. (a) The experimental and fitting results of the nickel layer thickness d_{Ni} dependence of V_{ISHE} . (b) The fitting result of the oscillation term V_{osc} . (c) The fitting result of the decay term V_{dec} .

than that of platinum in a similar situation, indicating that nickel is a potential high-efficiency spin-charge conversion material. Here, we should note that the spatial oscillation of spin originates from the ferromagnetic Fermi surface structure, which does not require a specific orientation of spin. In previous theoretical work [10,14], the spin-polarization direction was intentionally designed to be noncollinear with the localized magnetic moment in order to ensure a nonzero STT intensity. In our work, the spatial spin oscillation is detected by the inverse spin Hall effect, making it permissible for the spin-polarization direction to be collinear with the magnetic moment. Moreover, in our spin-pump setup, the ISHE signal reaches the maximum value when the external magnetic field is aligned with the in-plane direction of the device.

Several important aspects of this study deserve attention. First, the results disclosed in this study are a groundbreaking discovery of quantum coherence between spins.

Nevertheless, this is not the first study to explore the thickness dependence of ISHE for nickel [30]. The lack of comparable oscillation observations in earlier studies by other researchers may be because of the differing qualities of nickel films used. The superior interface and bulk quality of the nickel films in our device afforded us the chance to observe spin current oscillation. Further, the thickness interval applied in other experiments, which is comparable to the oscillation period, could have led them to overlook this oscillation. Second, as shown in Fig. 4(a), we notice that when the thickness of nickel falls below 4 nm, the spatial oscillation does not entirely correspond with our theoretical predictions. This divergence can mainly be ascribed to two factors. First, thin nickel films are inherently different from bulk nickel, a variation that results in the distinctive band structure of ultrathin nickel films, which might induce fluctuations in the oscillation period and amplitude. Moreover, at thicknesses lower than 4 nm, the interface and surface might render the first three data points unreliable due to the induction of extra scattering in the direction of the inverse spin Hall current. During the data-fitting process, we focused primarily on data points post-4-nm thickness, denoting data points before 4 nm with dashed lines. It is noteworthy that discernible oscillations are still detectable even at data points below 4 nm, thereby affirming the continued presence of spin coherence.

IV. SUMMARY

In summary, the high quality of devices allows the detection of an oscillation of ISHE signals in a series of ultrathin nickel films. This spatial oscillation of spin currents is attributed to the spin coherence between majority and minority spins in the nickel. The estimated wavelength corresponds well with the theoretical prediction of spin-coherence wavelength. This work reveals previously neglected details of spin transport and may inspire new ideas about spin devices, such as modulating the spin quantum state itself by altering the Fermi surface of the magnetic system to create new functional devices like a tunable spin oscillator.

ACKNOWLEDGMENTS

Z. Q. acknowledges support from the National Natural Science Foundation of China (Grant No. 52171173). D. H. acknowledges the support from the National Key R&D Program under Grant No. 2022YFA1403502, and the National Natural Science Foundation of China (Grant No. 12234017, No. 12074366).

- [1] M. N. Baibich, J. M. Broto, A. Fert, F. Nguyen Van Dau, F. Petroff, P. Etienne, G. Creuzet, A. Friederich, and J. Chazelas, *Giant magnetoresistance of (001)Fe/(001)Cr magnetic superlattices*, *Phys. Rev. Lett.* **61**, 2472 (1988).

- [2] G. Binasch, P. Grünberg, F. Saurenbach, and W. Zinn, *Enhanced magnetoresistance in layered magnetic structures with antiferromagnetic interlayer exchange*, *Phys. Rev. B* **39**, 4828 (1989).
- [3] E. Y. Tsymlal, O. N. Mryasov, and P. R. LeClair, *Spin-dependent tunnelling in magnetic tunnel junctions*, *J. Phys. Condens. Matter* **15**, R109 (2003).
- [4] A. Hirohata and K. Takanashi, *Future perspectives for spintronic devices*, *J. Phys. D* **47**, 193001 (2014).
- [5] L. Berger, *Emission of spin waves by a magnetic multilayer traversed by a current*, *Phys. Rev. B* **54**, 9353 (1996).
- [6] E. Myers, D. C. Ralph, J. A. Katine, R. N. Louie, and R. A. Buhrman, *Current-induced switching of domains in magnetic multilayer devices*, *Science* **285**, 867 (1999).
- [7] L. Liu, Chi-Feng Pai, Y. Li, H. W. Tseng, D. C. Ralph, and R. A. Buhrman, *Spin-torque switching with the giant spin Hall effect of tantalum*, *Science* **336**, 555 (2012).
- [8] I. M. Miron, K. Garello, G. Gaudin, P.-J. Zermatten, M. V. Costache, S. Auffret, S. Bandiera, B. Rodmacq, A. Schuhl, and P. Gambardella, *Perpendicular switching of a single ferromagnetic layer induced by in-plane current injection*, *Nature (London)* **476**, 189 (2011).
- [9] M. D. Stiles and J. Miltat, *Spin-transfer torque and dynamics*, in *Spin Dynamics in Confined Magnetic Structure III*, edited by B. Hillebrands and K. Ounadjela (Springer, New York, 2006), pp. 225–308.
- [10] M. D. Stiles and A. Zangwill, *Anatomy of spin-transfer torque*, *Phys. Rev. B* **66**, 014407 (2002).
- [11] D. L. Mills, *Ferromagnetic resonance relaxation in ultrathin metal films: The role of the conduction electrons*, *Phys. Rev. B* **68**, 014419 (2003).
- [12] A. Brataas, G. E. W. Bauer, and P. J. Kelly, *Non-collinear magnetoelectronics*, *Phys. Rep.* **427**, 157 (2006).
- [13] K. Carva and I. Turek, *Spin-mixing conductances of thin magnetic films from first principles*, *Phys. Rev. B* **76**, 104409 (2007).
- [14] S. Wang, Y. Xu, and K. Xia, *First-principles study of spin-transfer torques in layered systems with noncollinear magnetization*, *Phys. Rev. B* **77**, 184430 (2008).
- [15] J. Yu *et al.*, *Long spin coherence length and bulk-like spin-orbit torque in ferrimagnetic multilayers*, *Nat. Mater.* **18**, 29 (2019).
- [16] A. A. Kovalev, G. E. W. Bauer, and A. Brataas, *Perpendicular spin valves with ultrathin ferromagnetic layers: Magnetoelectronic circuit investigation of finite-size effects*, *Phys. Rev. B* **73**, 054407 (2006).
- [17] P. G. De Gennes, *Boundary effects in superconductors*, *Rev. Mod. Phys.* **36**, 225 (1964).
- [18] L. N. Bulaevskii, O. V. Dolgov, and M. O. Pttitsyn, *Properties of strong-coupled superconductors*, *Phys. Rev. B* **38**, 11290 (1988).
- [19] J. Barnaś, A. Fert, M. Gmitra, I. Weymann, and V. K. Dugaev, *From giant magnetoresistance to current-induced switching by spin transfer*, *Phys. Rev. B* **72**, 024426 (2005).
- [20] M. Zwierzycki, Y. Tserkovnyak, P. J. Kelly, A. Brataas, and G. E. W. Bauer, *First-principles study of magnetization relaxation enhancement and spin transfer in thin magnetic films*, *Phys. Rev. B* **71**, 064420 (2005).
- [21] Y. H. Zhu, B. Hillebrands, and H. C. Schneider, *Spin-signal propagation in time-dependent noncollinear spin transport*, *Phys. Rev. B* **79**, 214412 (2009).
- [22] H. Ohno, *Properties of ferromagnetic III-V semiconductors*, *J. Magn. Magn. Mater.* **200**, 110 (1999).
- [23] F. Matsukura, H. Ohno, and T. Dietl, *III-V ferromagnetic semiconductors*, in *Handbook of Magnetic Materials*, edited by K. H. L. Buschow (Elsevier, New York, 2002), pp. 1–87.
- [24] Z. Qiu, T. An, K. Uchida, D. Hou, Y. Shiomi, Y. Fujikawa, and E. Saitoh, *Experimental investigation of spin Hall effect in indium tin oxide thin film*, *Appl. Phys. Lett.* **103**, 182404 (2013).
- [25] E. Saitoh, M. Ueda, H. Miyajima, and G. Tatara, *Conversion of spin current into charge current at room temperature: Inverse spin-Hall effect*, *Appl. Phys. Lett.* **88**, 182509 (2006).
- [26] K. Ando *et al.*, *Inverse spin-Hall effect induced by spin pumping in metallic system*, *J. Appl. Phys.* **109**, 103913 (2011).
- [27] P. Scherrer, *Bestimmung der grösse und der inneren struktur von kolloidteilchen mittels röntgenstrahlen*, *Nachr. Ges. Wiss. Göttingen* **26**, 98 (1918).
- [28] M. Khatami, L. H. Omari, N. Eazizayene, and H. Lassri, *Temperature dependence of the electrical resistivity of amorphous $\text{Co}_{80-x}\text{Er}_x\text{B}_{20}$ alloys: Localization and electron-electron interaction effects*, *J. Low Temp. Phys.* **195**, 211 (2019).
- [29] See Supplemental Material at <http://link.aps.org/supplemental/10.1103/PhysRevX.14.021045> for spin oscillation behaviors for a broad temperature range.
- [30] C. Du, H. Wang, F. Yang, and P. C. Hammel, *Systematic variation of spin-orbit coupling with d-orbital filling: Large inverse spin Hall effect in 3d transition metals*, *Phys. Rev. B* **90**, 140407(R) (2014).